

Supplementary Figures and Tables

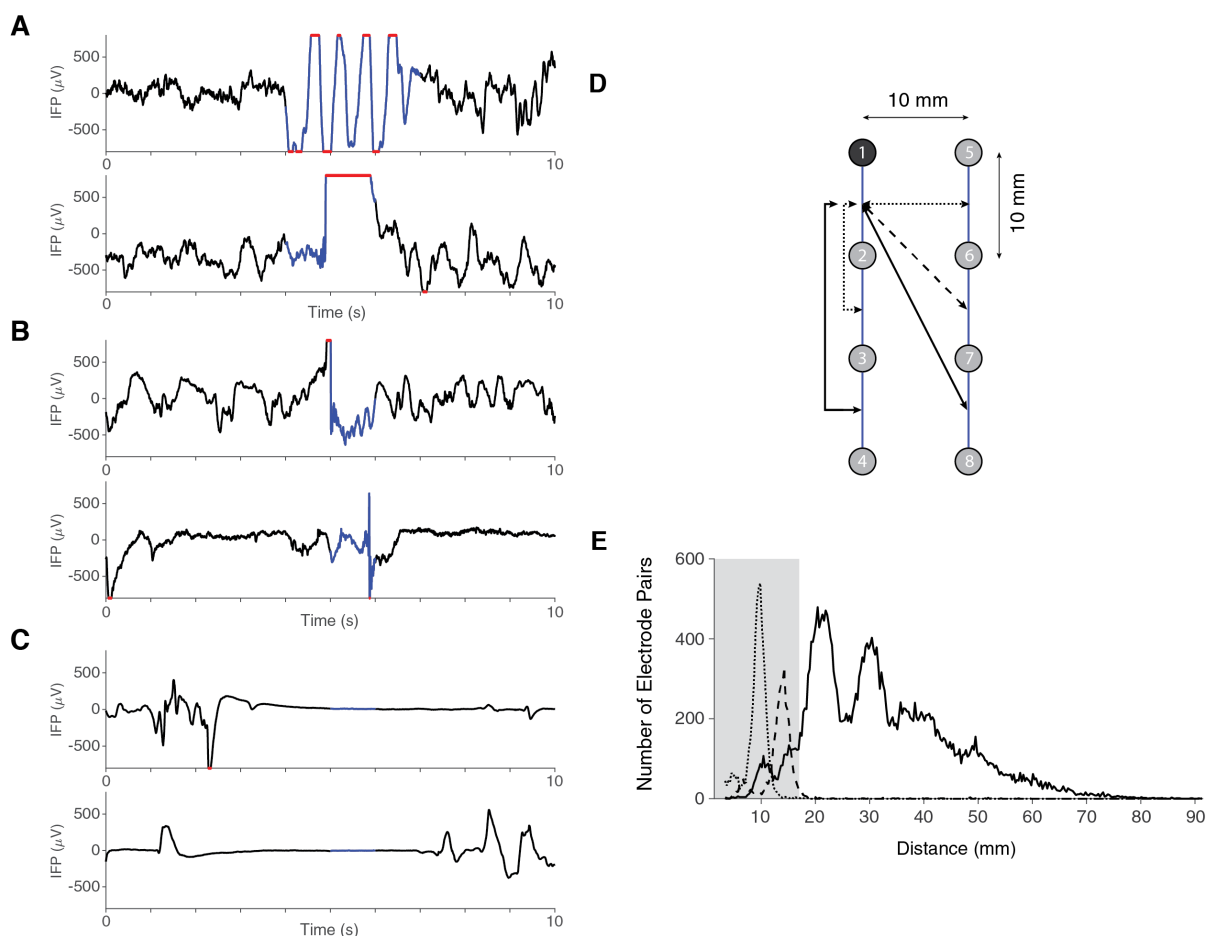


Figure S1, related to Figure 1. Examples of artifacts and nearby electrodes removed from analyses. Artifacts were detected according to 3 criteria (**STAR Methods**), and removed from analyses. We present 2 example 10-second segments from 2 electrodes for each criterion (artifacts are marked by blue lines superimposed on the IFP voltage traces shown in black, out-of-range points are indicated in red). **(A)** Large amplitude events where $\max[V(t)] - \min[V(t)] > 2000 \mu\text{V}$ (0.72% of total events). Red markers indicate time points where the voltage values were out of the scale chosen here for illustration purposes only ($\pm 800 \mu\text{V}$). **(B)** Large slope events where the maximum rate of change in voltage over time exceeded a threshold of $100 \mu\text{V}/\text{ms}$ (0.44% of total events). **(C)** Low amplitude events where $\max[V(t)] - \min[V(t)] < 10 \mu\text{V}$ (0.10% of total events). In total, 2.1% of the data were marked as potential artifacts (95-percentile range across subjects: 1.4% to 11%). **(D)** Example schematic layout of 8 physical electrodes shown on a 4 by 2 grid. The blue lines show pairs of electrodes used for bipolar referencing (**STAR Methods**). Focusing on electrode 1 (top left), the voltage was calculated with respect to electrode number 2. Here we show all five possible pairs for this electrode. Adjacent neighbors (dotted lines) and diagonal neighbors (dashed line) were excluded from analyses. The two remaining interactions (solid lines) were included in the analyses. **(E)** Histogram of the distance between electrodes that were adjacent neighbors (dotted line), diagonal neighbors (dashed line), or otherwise (solid line). The shaded region indicates pairs of bipolar-referenced electrodes that were less than 17 mm apart, which were excluded from analyses (**STAR Methods**). The peaks at 20 and 30 mm reflect the typical geometry of electrode grids and strips.

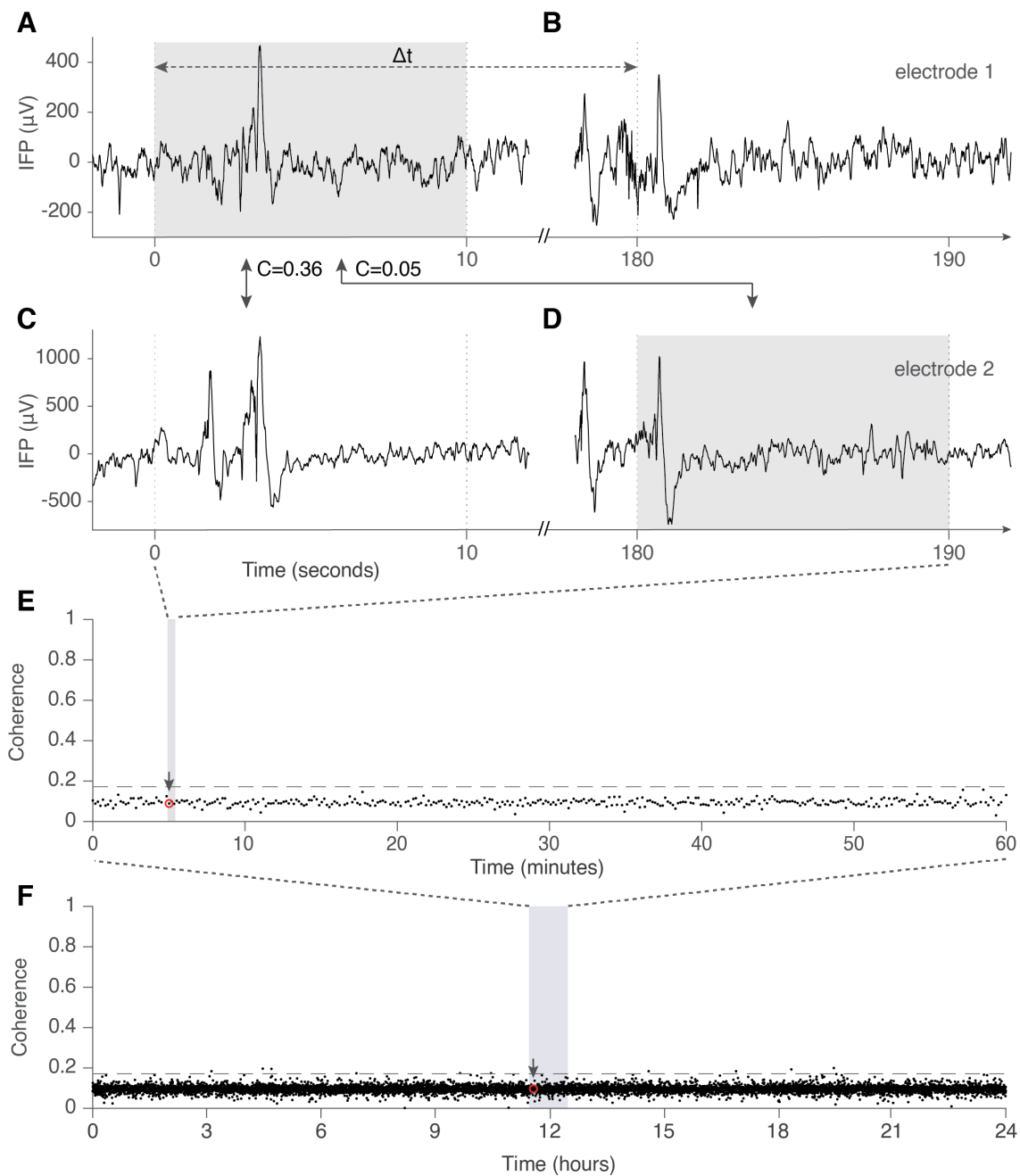


Figure S2, related to Figure 2. Null hypothesis defined by temporally shifting neural signals. Segments of data from two electrodes (A-B: electrode 1, C-D: electrode 2). The segment in (A) was simultaneously recorded with the segment shown in (C). The coherence between these two segments was 0.36. We considered a random time shift Δt , in this case, $\Delta t = 180$ seconds (note the cut along the x-axis). The coherence between the segment in (A) and the one in (D) was 0.05. Electrode locations are the same as in Figure 2A. (E-F) The same procedure was repeated at each time point using random values of Δt , leading to the distribution of coherence values under the null hypothesis for 24 hours in (F), and the zoomed-in one-hour segment in (E). The horizontal dashed lines indicate the significance threshold $C=0.17$ (STAR Methods). The arrows in (E) and (F) indicate the example coherence between the (A) and (D) segments.

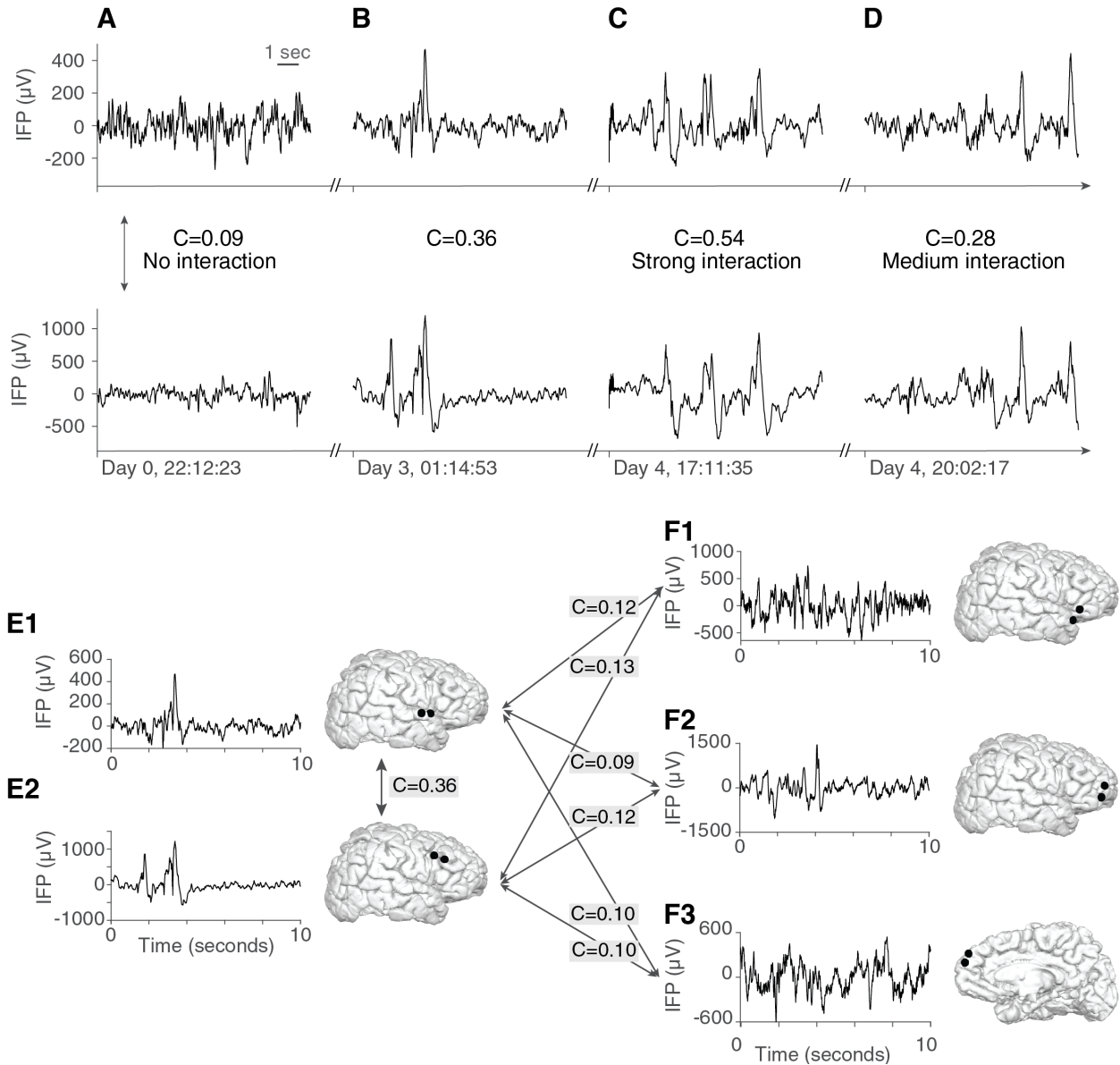


Figure S3, related to Figure 2. Coherence values change over time and show spatial specificity. Following the format in **Figure 2**, here we show four 10-second segments spanning multiple days from the same two cortical areas (top: right Superior Temporal gyrus; bottom: right Pars Opercularis) (note cut along the x-axis). **(A)** Non-significant coherence ($C=0.09$), **(B)** Segment shown in **Figure 2A** ($C=0.36$). **(C)** High coherence segment ($C=0.54$). **(D)** Medium coherence segment ($C=0.28$). **(E)** Reproduction of **Figure 2A** in the main text for comparison. The coherence between the two bipolar electrode pairs in this segment was 0.36. **(F)** Three bipolar electrode pairs located in the left superior temporal gyrus, left rostral middle frontal gyrus, and left post-central gyrus, simultaneously recorded with the ones in **(E1/E2)**. None of the 6 coherence values between **(E1/E2)** and **(F1/F2/F3)** were statistically significant.

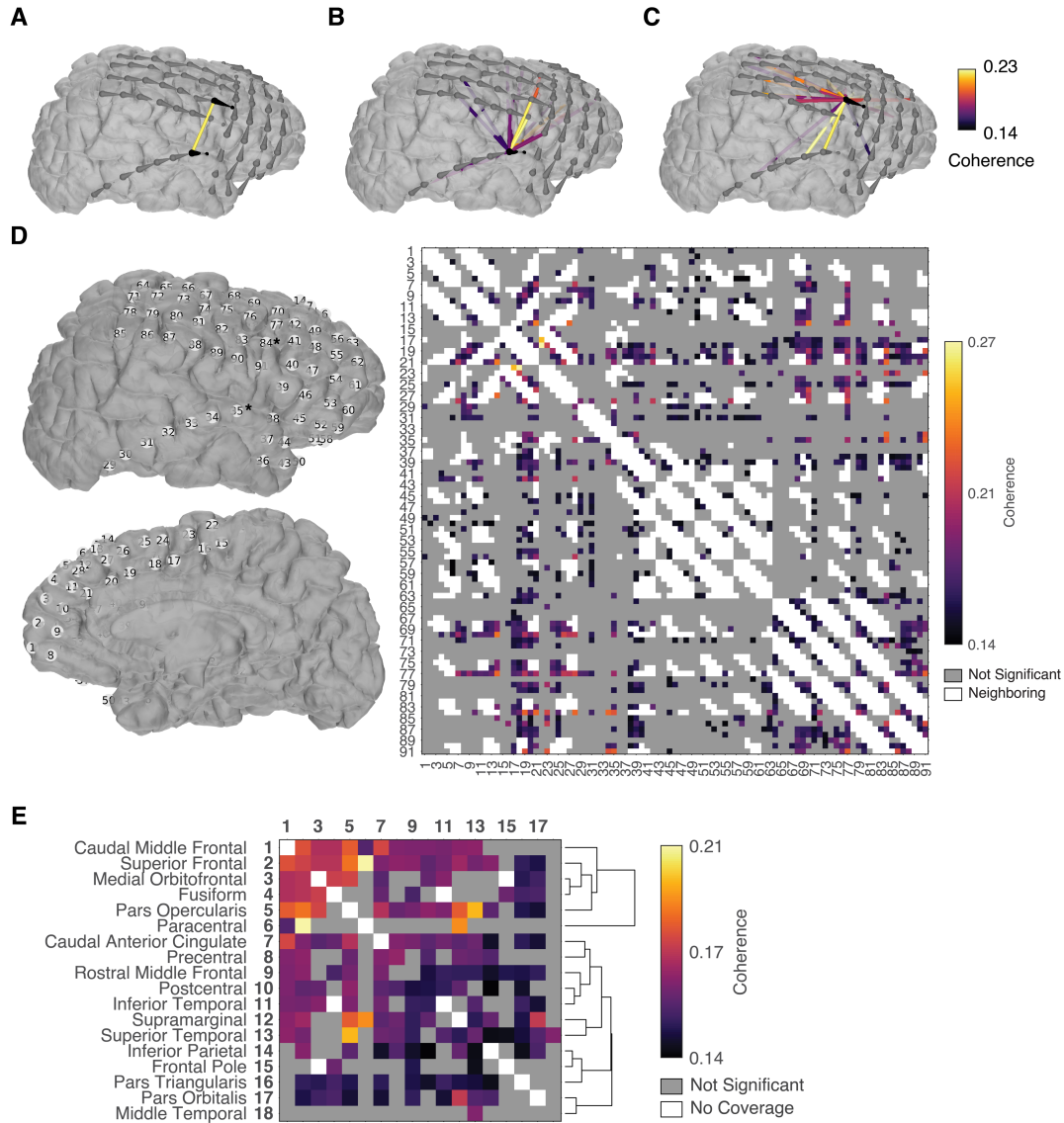


Figure S4, related to Figure 4. Time-averaged coherence values show spatial specificity. All interactions shown here are measured by the time-averaged coherence in subject 3 for 5.5 days. Bipolar electrode pairs are indicated by the droplet-shaped markers where the head indicates the primary electrode and the tail points to the ground electrode. **(A)** The bipolar pair from **Figure 2A** is indicated in black. The time-averaged coherence was 0.22 and is represented by a colored line connecting the two bipolar electrode positions (dark circles, other bipolar electrodes are denoted by light circles). **(B)** All interactions with the electrode in the Superior Temporal gyrus from **(A)**. **(C)** All interactions with the electrode in the Pars Opercularis from **(A)**. **(D)** Interactions shown for all 91 electrodes in this subject (see electrode locations on the left and color scale on the right). Of the 4,095 total possible pairwise combinations, 3,193 pairs satisfied the distance constraint (**Figure S2**). A total of 557 pairs (17%) showed statistically significant and temporally consistent interactions. **(E)** Interactions shown between all electrode pairs in this subject mapped onto the brain areas defined by the Desikan-Killiany parcellation ([Desikan et al., 2006](#)). The dendrogram shows relationships between areas, based on their similarities in coherence values. The interaction between the Superior Temporal gyrus and Pars Opercularis (**A**) can be found in row 5, column 13.

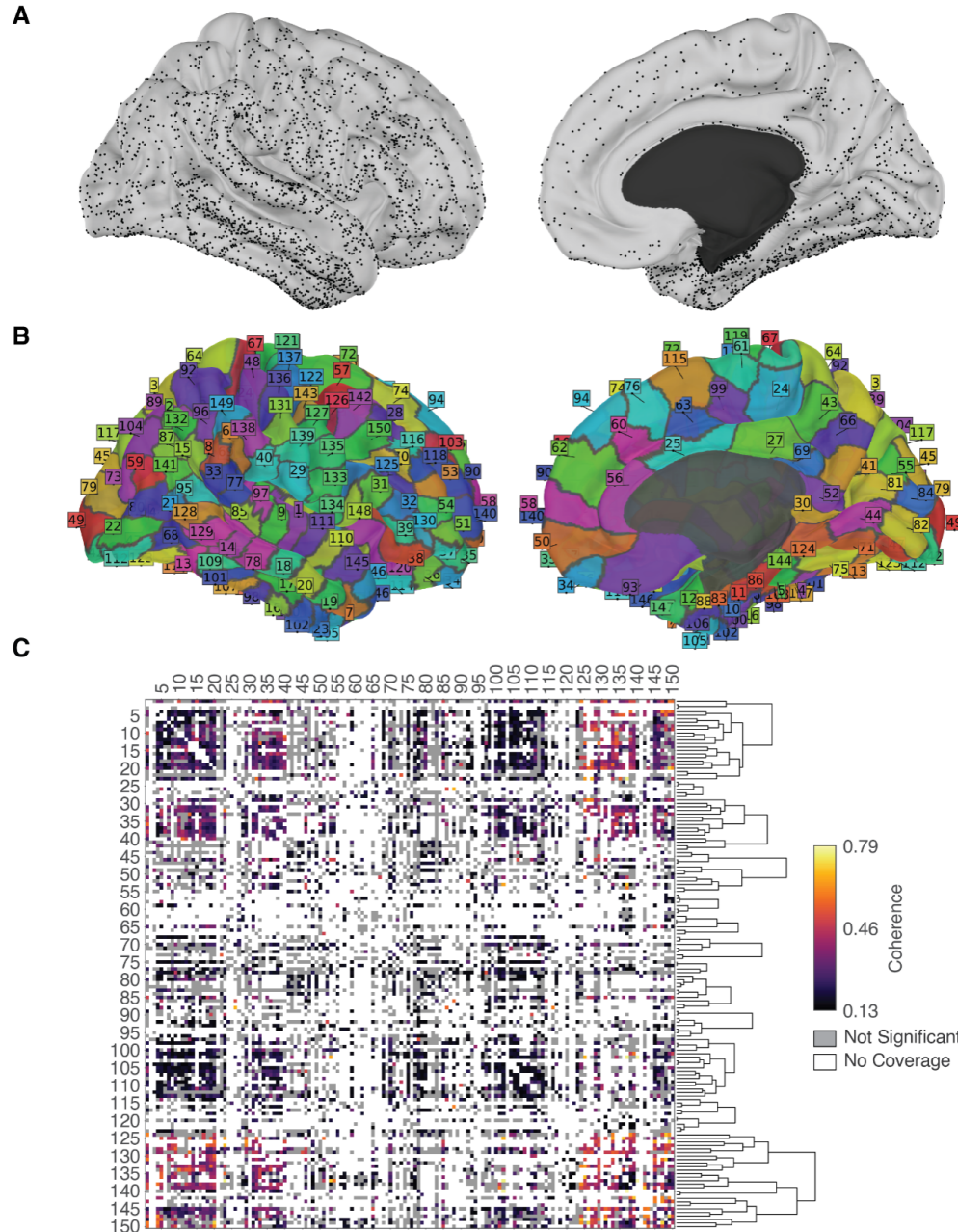


Figure S5, related to Figure 5. Parcellation of the human brain into 150 areas based on electrode coverage. **A.** All 3,615 bipolar electrode locations shown as black dots on average pial surface of the right hemisphere. The lateral (left) and medial (right) views are shown. **(B)** Each of the 150 areas obtained by clustering electrode distances is represented as a colored patch on the surface, separated by areal boundaries in dark gray (**STAR Methods**). **(C)** Interactions between areas in the 150-area parcellation. Interactions shown were significant in at least 2 subjects and at least 10 electrode pairs. The fraction of pairs of brain areas that did not have adequate coverage was 58% (6,531 of 11,175). Of the pairs of brain areas that had adequate coverage, 51% (2,387 of 4,644) showed statistically significant interactions. Region numbers correspond to those shown in **B**. The example electrodes from Subject 3 in **Figure 2A** were localized to areas 111 and 148, which showed significant overlap with Desikan-Killiany areas Superior Temporal gyrus and Pars Opercularis, respectively.

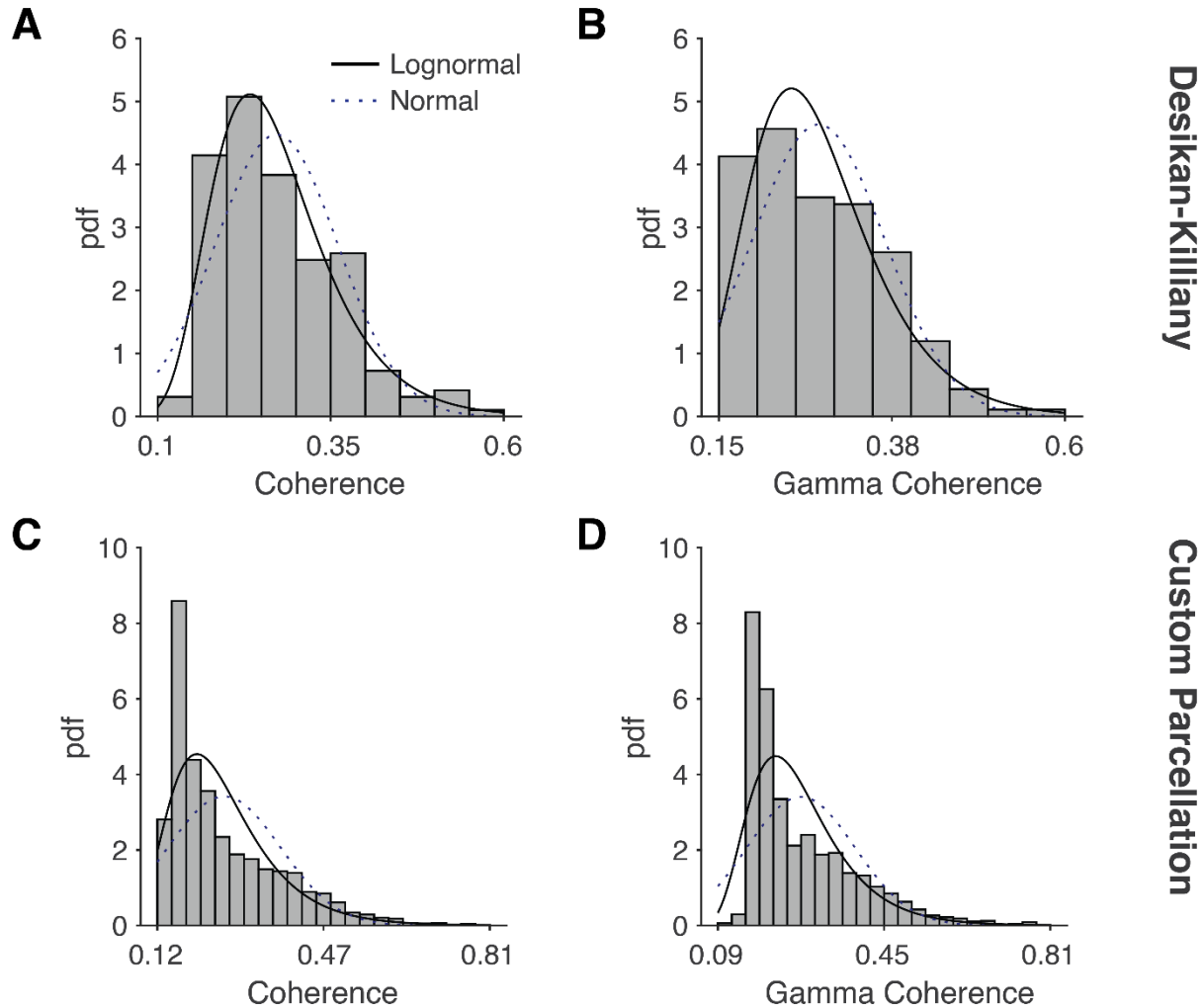


Figure S6, related to Figure 5. Log-normal distributions of physiological interaction coherence values. (A) Histogram of the 193 significant broadband coherence values from **Figure 5**. The log-normal fit is indicated by the solid line, the normal fit is indicated by the blue dotted line. (B) Histogram and log-normal fit for the 184 significant coherence values calculated in the gamma frequency band (see Supplementary Website: <http://www.braininteractome.com/>). (C) Histogram of the 2,387 significant broadband coherence values between areas defined by the custom 150-area parcellation from **Figure S5C**. (D) Histogram of the 2,110 significant gamma band coherence values defined by the custom 150-area parcellation (see Supplementary Website <http://www.braininteractome.com/>).

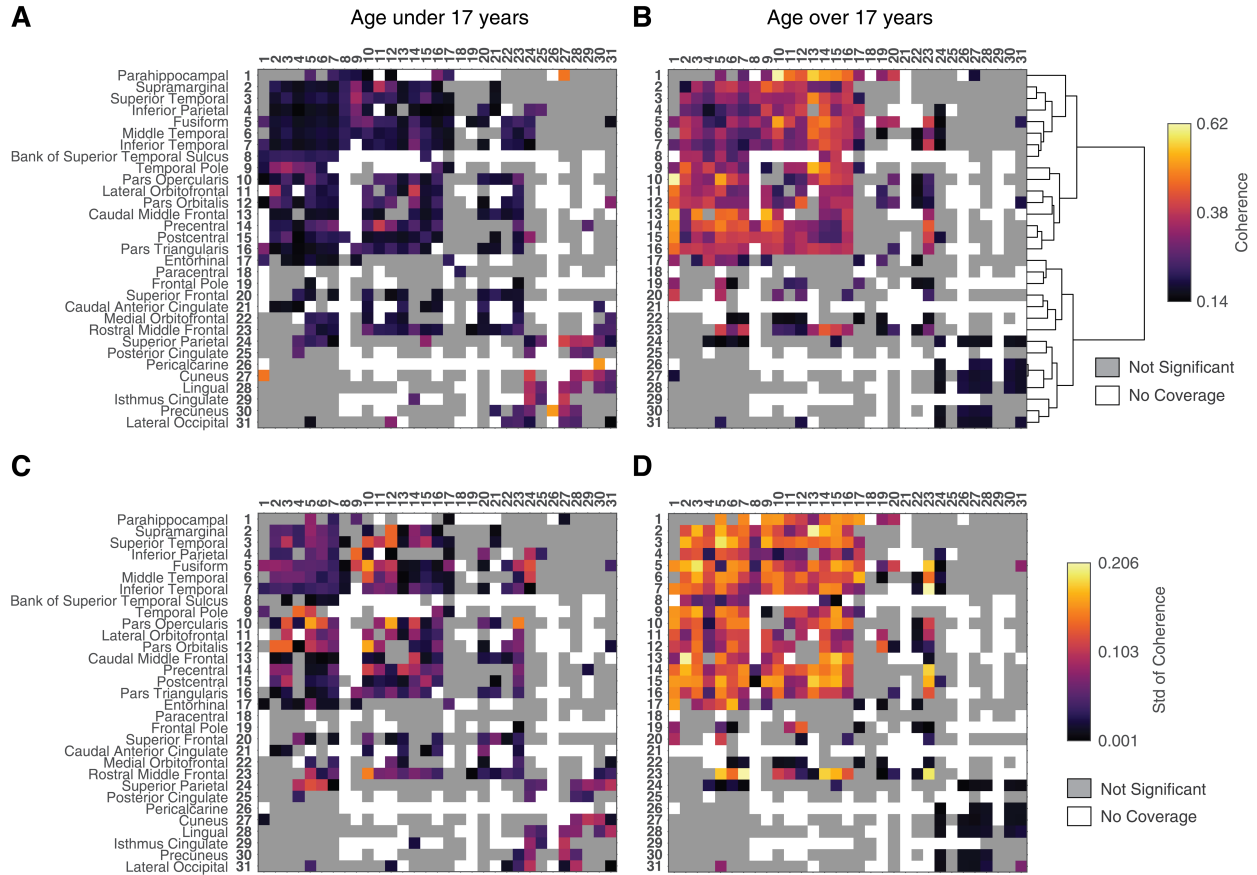


Figure S7, related to Figure 5. The effects of age on coherence between Desikan areas. All subjects were split into two equal-sized groups: below 17 years old (**A**) and above 17 years old (**B**). Following the format from **Figure 5**, this figure shows interactions between all brain areas for these two groups. The standard deviations of coherence values are shown in (**C**) and (**D**) for the corresponding age groups.

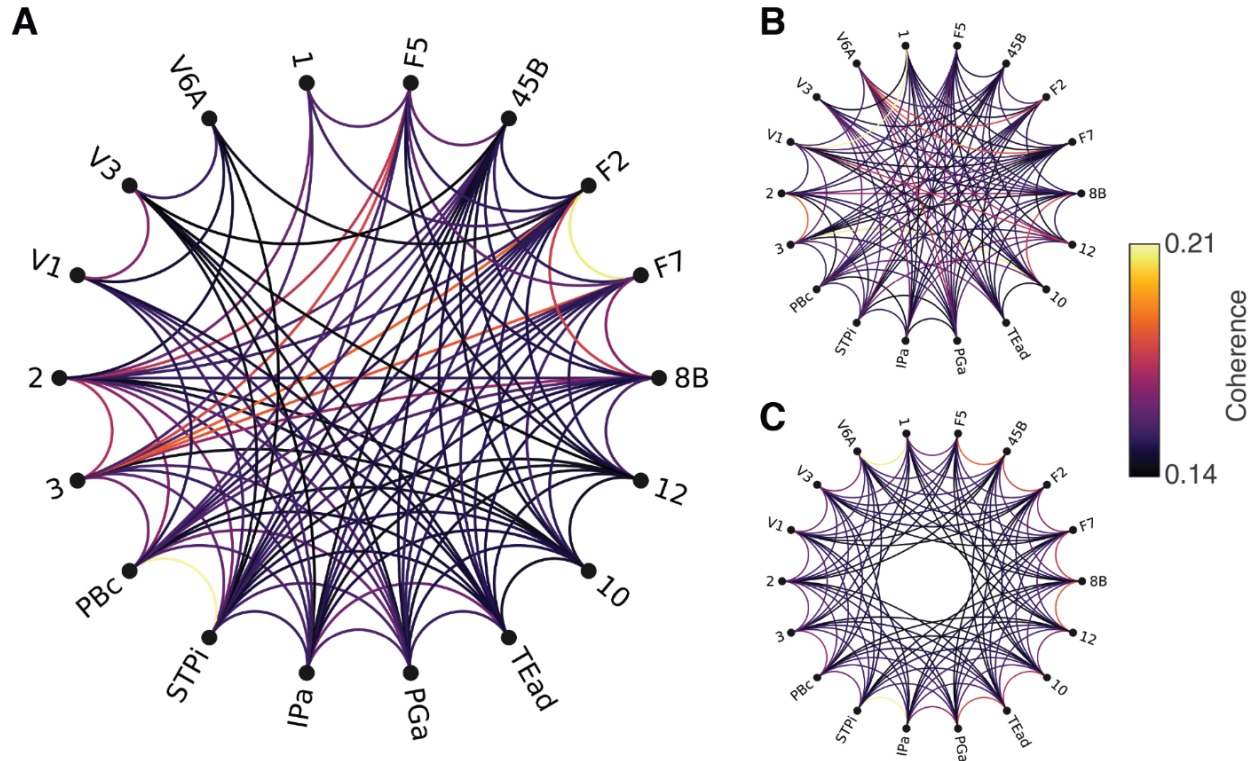


Figure S8, related to Figure 6. The macaque monkey physiological interactivity small-world network. Following the format from **Figure 6**, here we show the physiological interaction network from recordings in macaque monkeys (**A**), the restructured random network (**B**), and the lattice network (**C**). The small-world coefficient ([Humphries and Gurney, 2008](#)) was $\sigma=1.15$ (95% CI: 1.09, 1.20), satisfying the small-world range $\sigma>1$. The small-world measurement ([Telesford et al., 2011](#)) was $\omega=-0.188$ (95% CI: -0.195, -0.182), satisfying the small-world range $-0.5<\omega<0.5$. Area names follow the original convention in the Markov-Kennedy parcellation ([Markov et al., 2012](#)).

Supplementary Tables

Subject	Age	Gender	Hemisphere	Handedness	Days	Electrodes	Bipolar Electrodes
1	21	M	L	R	6.0	72	63
2	14	M	L	R	5.6	72	63
3	3	F	R	R	5.5	104	91
4	32	M	R	R	6.4	72	63
5	46	F	L	R	3.5	72	63
6	10	F	L	R	4.3	88	77
7	20	F	R	R	5.1	88	77
8	39	F	R	R	7.0	72	63
9	47	M	R	R	5.6	48	42
10	21	M	R	L	5.8	70	61
11	26	M	R	R	2.0	72	63
12	18	M	R	R	5.2	64	56
13	9	F	L	R	5.2	72	63
14	32	M	R	L	3.8	40	35
15	21	M	L	R	7.5	72	63
16	8	M	L	L	4.5	128	112
17	10	F	L	R	6.4	104	91
18	9	M	R	R	3.8	104	91
19	18	F	L	R	6.5	120	105
20	15	M	R	R	5.1	80	70
21	12	M	R	R	6.2	104	91
22	17	F	L	R	6.6	56	49
23	9	F	R	R	6.6	88	77
24	16	M	R	R	4.6	104	91
25	9	M	R	R	2.7	104	91
26	17	F	L,R	R	10.4	104	91
27	3	M	L	R	6.8	88	77
28	11	F	L	R	6.6	72	63
29	19	M	L	R	3.7	128	112
30	44	M	R	R	2.4	26	20
31	31	M	R	R	7.3	34	27
32	42	F	R	R	4.3	38	32
33	18	M	R	R	8.8	88	77
34	31	M	L	R	3.8	75	65
35	16	M	L	R	1.3	88	77
36	18	F	L	R	5.1	88	77
37	18	M	L	R	3.1	72	63
38	19	F	L	R	5.7	120	105
39	11	M	L	L	5.6	104	91
40	17	F	R	R	5.2	176	154
41	31	F	L	R	4.6	79	68
42	16	F	L	R	4.6	96	84
43	13	M	L	L	5.7	92	80
44	14	F	L	R	6.4	72	63
45	10	F	R	R	0.9	112	98
46	7	M	L	R	7.8	120	105
47	10	M	R	R	6.4	120	105
48	17	M	R	R	1.7	80	70

Table S1, related to Figure 1. List of subjects (n = 48). Age, gender, handedness, and left/right hemisphere coverage are shown with the number of days of continuous intracranial field potential (IFP) recordings, number of electrodes, and number of bipolar electrodes (see **STAR Methods** for bipolar electrode definition).

Criterion	Total	Mean (n=48)	Standard deviation	Minimum	Maximum
Amplitude, large (i)	0.72%	0.71%	1.4%	<0.01%	5.9%
Slope (ii)	0.44%	0.38%	0.63%	<0.01%	3.6%
Amplitude, small (iii)	0.10%	0.13%	0.45%	0%	2.9%
Events (iv)	0.49%	0.68%	1.8%	0%	10.5%
Electrodes (v)	0.34%	0.36%	0.36%	<0.01%	1.4%
Total	2.1%	2.3%	2.6%	<0.01%	12.1%

Table S2, related to Figure 1. Percentage of artifacts removed according to each criterion (see **STAR Methods** for definitions and **Figure S1** for illustration of the different types of artifacts). The total fraction of observed 1-second segments of IFP recordings marked as artifacts. Segments could satisfy more than one criterion, with the exception of (i) and (iii). The overall fraction of annotated artifacts was 2.1%.

Desikan-Killiany Region	Abbreviation	Alias	Bipolar Electrodes	(%)	Left Hemisphere	Right Hemisphere
Middle Temporal	MTP	middletemporal	462	12.8%	297	165
Inferior Temporal	ITP	inferiortemporal	399	11.0%	263	136
Superior Temporal	STP	superiortemporal	330	9.1%	200	130
Fusiform	FUS	fusiform	266	7.4%	185	81
Rostral Middle Frontal	RMF	rostralmiddlefrontal	220	6.1%	97	123
Lateral Occipital	LOC	lateraloccipital	174	4.8%	90	84
Supramarginal	SMA	supramarginal	171	4.7%	84	87
Precentral	PRC	precentral	155	4.3%	60	95
Postcentral	PSC	postcentral	140	3.9%	52	88
Inferior Parietal	IPA	inferiorparietal	127	3.5%	47	80
Superior Frontal	SFR	superiorfrontal	117	3.2%	28	89
Lingual	LIN	lingual	115	3.2%	44	71
Lateral Orbitofrontal	LOF	lateralorbitofrontal	112	3.1%	71	41
Entorhinal	ENT	entorhinal	96	2.7%	69	27
Temporal Pole	TPP	temporalpole	83	2.3%	40	43
Pars Opercularis	POP	parsopercularis	80	2.2%	42	38
Precuneus	PCU	precuneus	75	2.1%	29	46
Pars Orbitalis	POR	parsorbitalis	71	2.0%	41	30
Pars Triangularis	PTR	parstriangularis	63	1.7%	44	19
Parahippocampal	PHC	parahippocampal	61	1.7%	52	9
Superior Parietal	SPA	superiorparietal	58	1.6%	17	41
Caudal Middle Frontal	CMF	caudalmiddlefrontal	49	1.4%	16	33
Cuneus	CUN	cuneus	38	1.1%	6	32
Isthmus Cingulate	ICN	isthmuscingulate	29	0.8%	14	15
Medial Orbitofrontal	MOF	medialorbitofrontal	28	0.8%	12	16
Paracentral	PCE	paracentral	23	0.6%	0	23
Posterior Cingulate	PCN	posteriorcingulate	21	0.6%	7	14
Frontal Pole	FRP	frontalpole	16	0.4%	7	9
Unknown	UNK	unknown	10	0.3%	5	5
Bank of Superior Temporal Sulcus	BST	bankssts	8	0.2%	4	4
Caudal Anterior Cingulate	CAC	caudalanteriorcingulate	7	0.2%	2	5
Pericalcarine	PCL	pericalcarine	6	0.2%	0	6
Corpus Callosum	CCA	corpuscallosum	3	0.1%	3	0
Rostral Anterior Cingulate	RAC	rostralanteriorcingulate	2	0.1%	0	2
Transverse Temporal	TVT	transversetemporal	0	0.0%	0	0
Insula	INS	insula	0	0.0%	0	0
		Total:	3615	100%	1928	1687

Table S3, related to Figure 1. Number of bipolar electrodes covering each area in the Desikan-Killiany parcellation ([Desikan et al., 2006](#)). Three-letter abbreviations (as shown in **Figure 6**) and their *freesurfer* names are shown with the number of bipolar electrodes localized to those areas. After applying the coverage criteria (see **STAR Methods**), 31 areas remained covered for physiological interaction network analyses (bolded).

	Broadband		Gamma Band	
	Monkeys	Humans	Monkeys	Humans
L	8.82	5.23	8.08	5.34
C	0.57	0.49	0.73	0.53
L_{random}	8.50 (0.03)	4.36 (0.03)	7.87 (0.02)	4.37 (0.03)
$L_{lattice}$	8.85 (0.01)	4.93 (0.004)	8.09 (0.004)	4.92 (0.004)
C_{random}	0.48 (0.01)	0.34 (0.01)	0.58 (0.01)	0.34 (0.01)
$C_{lattice}$	0.49 ($6 \cdot 10^{-5}$)	0.40 ($6 \cdot 10^{-5}$)	0.59 ($4 \cdot 10^{-5}$)	0.42 ($2 \cdot 10^{-5}$)
σ	1.1 (0.03)	1.2 (0.03)	1.2 (0.03)	1.3 ($5 \cdot 10^{-2}$)
ω	-0.19 (0.003)	-0.41 (0.01)	-0.26 (0.002)	-0.44 (0.006)

Table S4, related to Figure 6. Small-world network measures. The characteristic pathlength (L) and clustering coefficient (C) are shown for human and macaque monkey physiological networks based on the broadband and gamma band coherence (see **STAR Methods**). Values shown represent means from multiple random initializations of random and lattice networks. Values shown in parentheses represent standard deviations. The small-world coefficient σ ([Humphries and Gurney, 2008](#)) and small-world measurement ω ([Telesford et al., 2011](#)) both indicated the presence of small-world networks across species and frequency bands.

Subject	L	C	L_{random}	$L_{lattice}$	C_{random}	$C_{lattice}$	σ	ω
1	2.60	0.99	2.60 (0.00)	2.83 (0.05)	0.83 (0.00)	0.73 (0.01)	1.20 (0.00)	-0.34 (0.02)
2	6.71	1.11	6.62 (0.05)	5.34 (0.03)	0.76 (0.01)	0.88 (0.00)	1.44 (0.01)	-0.28 (0.01)
5	5.55	0.83	5.37 (0.10)	4.60 (0.00)	0.58 (0.07)	0.73 (0.00)	1.39 (0.17)	-0.18 (0.02)
7	7.31	1.29	7.30 (0.02)	6.22 (0.02)	0.80 (0.00)	0.97 (0.00)	1.60 (0.01)	-0.32 (0.01)
10	4.36	0.88	4.39 (0.05)	3.61 (0.00)	0.70 (0.08)	0.80 (0.00)	1.30 (0.16)	-0.10 (0.01)
13	3.28	0.81	3.25 (0.04)	3.24 (0.01)	0.61 (0.08)	0.53 (0.00)	1.35 (0.19)	-0.55 (0.01)
15	6.23	0.82	6.20 (0.10)	5.31 (0.01)	0.56 (0.08)	0.72 (0.00)	1.51 (0.23)	-0.14 (0.02)
16	7.08	0.93	8.39 (0.02)	6.97 (0.00)	0.69 (0.05)	0.88 (0.00)	1.61 (0.11)	0.13 (0.00)
25	4.15	0.83	4.66 (0.08)	4.57 (0.01)	0.46 (0.06)	0.51 (0.00)	2.06 (0.27)	-0.49 (0.02)
34	2.03	1.00	2.03 (0.00)	2.08 (0.01)	0.87 (0.00)	0.84 (0.00)	1.15 (0.00)	-0.19 (0.00)
40	9.78	0.71	8.73 (0.11)	8.47 (0.01)	0.39 (0.04)	0.48 (0.00)	1.64 (0.18)	-0.59 (0.01)
41	3.11	0.74	3.10 (0.01)	3.13 (0.01)	0.73 (0.01)	0.60 (0.00)	1.01 (0.01)	-0.23 (0.00)
48	7.19	1.30	7.19 (0.00)	7.16 (0.00)	0.99 (0.00)	0.99 (0.00)	1.31 (0.00)	-0.31 (0.00)

Table S5, related to Figure 6. Small-world network measures in individual subjects. Small-world coefficients for 13 subjects with sufficient data following the format in **Table S4**. The coefficient σ ([Humphries and Gurney, 2008](#)) indicated the presence of a small-world network in all 13 subjects. The measurement ω ([Telesford et al., 2011](#)) indicated the presence of a small-world network in 11 of 13 subjects.

	Coherence	Pearson Correlation
L	5.23	3.27
C	0.49	0.71
L_{random}	4.36 (0.03)	3.07 (0.01)
$L_{lattice}$	4.93 (0.004)	2.99 (0.001)
C_{random}	0.34 (0.01)	0.38 (0.02)
$C_{lattice}$	0.40 ($6 \cdot 10^{-5}$)	0.53 ($5 \cdot 10^{-5}$)
σ	1.2 (0.03)	1.77 (0.10)
ω	-0.41 (0.01)	-0.40 (0.004)

Table S6, related to Figure 6. Small-world network measures are similar when using Coherence or Pearson correlation as a metric. Following the format in **Table S4**, here we show small-world network properties of the graph formed using the Pearson correlation coefficient as an alternative to the coherence. The small-world coefficient σ ([Humphries and Gurney, 2008](#)) and small-world measurement ω ([Telesford et al., 2011](#)) both indicated the presence of small-world networks.